PROCEEDINGS OF SCIENCE

Anisotropy search in the Ultra High Energy Cosmic Ray Spectrum in the Northern Hemisphere using the Telescope Array surface detector

T. Nonaka[∗a], **R. Cady**[b], **M. Fukushima**[a,c], **D. Ivanov**[b], **K. Kawata**[a], **E. Kido**[a], **J.N. Matthews**[b], **S. Nagataki**[d], **T. Okuda**[e], **H. Sagawa**[a], **N. Sakurai**[f], **B.T. Stokes**[b], **M. Takeda**[a] **and A. Taketa**[g], **for The Telescope Array Collaboration**[†]

[a] *Institute for Cosmic Ray Research, University of Tokyo, Kashiwa, Chiba, Japan*
[b] *High Energy Astrophysics Institute and Department of Physics and Astronomy, University of Utah, Salt Lake City, Utah, USA*
[c] *Kavli Institute for the Physics and Mathematics of the Universe (WPI), Todai Institutes for Advanced Study, the University of Tokyo, Kashiwa, Chiba, Japan*
[d] *Astrophysical Big Bang Laboratory, RIKEN, Wako, Saitama, Japan*
[e] *Department of Physical Sciences, Ritsumeikan University, Kusatsu, Shiga, Japan*
[f] *Graduate School of Science, Osaka City University, Osaka, Osaka, Japan*
[g] *Earthquake Research Institute, University of Tokyo, Bunkyo-ku, Tokyo, Japan*
E-mail: nonaka@icrr.u-tokyo.ac.jp

The Telescope Array (TA) experiment is located in the western desert of Utah, USA and observes ultra high energy cosmic rays in the northern hemisphere. In the highest part of the energy region, the cosmic ray energy spectrum shape carries information of the source density distribution. We search for directional differences in the energy spectrum shape. In this study, observed cosmic ray energy distributions are compared between sky areas that contain more nearby objects, such as the super-galactic plane, and others that do not.

The 34th International Cosmic Ray Conference,
30 July- 6 August, 2015
The Hague, The Netherlands

∗Speaker.
†For full author list and acknowledgments see http://www.telescopearray.org/images/papers/ICRC2015-authorlist.pdf

1. Introduction

Extragalactic objects with large volumes or very strong magnetic fields can be sources of acceleration of UHECR. At highest energy range, cosmic ray nuclei lose their energy in propagation through distances from a few Mpc to 100 Mpc. Since the attenuation length of cosmic ray depends on particle types, energy deposition in propagation depending on chemical composition. Proton which have energy $10^{19.7}$ eV interact with cosmic microwave background (CMB) photons and lose their energy generating pion. Then the spectrum of proton cosmic ray is expected to show suppression of the flux which is known as GZK cut off [1, 2]. Another process for proton is $e^+ + e^-$ creation from protons interacting with CMB photons. By this process, protons lose energies at around $10^{18.6}$ eV. Then, there is a chance to see difference of energy spectrum more explicitly by comparing the spectrum obtained from the area in celestial sphere which contain near objects and the one which does not contain near objects. Unlike usual anisotropy study, the detail of anisotropy comes from the spectrum modulation can be studied.

2. Experiment and analysis

Telescope Array(TA) experiment [3] is a hybrid detector which observe cosmic rays have energy $E > 10^{18}$ eV using fluorecence telescopes and surface detector. The surface detector consists of 507 scintillation counters deployed on a square grid with 1.2 km spacing, covering an area of 670 km^2 of area for detecting UHECR [4]. The operation of the surface detector started in 2008. The duty cycle of the observation is 95% on average. Now the exposure is the largest in the northern hemisphere. In this analysis, cosmic-ray events with energies greater than 10^{19} eV collected in a period from May 2008 to May 2013 are used to search for anisotropy in cosmic-ray energy spectrum. From Monte Carlo simulation, the trigger efficiency of cosmic-ray showers at zenith angles of less than 55° reaches 100% in the energy range greater than 10^{19} eV. The estimated energy resolution of reconstructed cosmic rays is about 20%, and the angular resolution is 2°[3, 5]. The distribution of zenith angles of the observed showers is shown in Fig. 1. In this analysis we divide the sky into two parts. One is the area that contains more nearby objects, whereas the other is the area that contains less nearby objects. The former is called the "**On source**" area, and the latter is called the "**Off source**" area. We performed two analyses defining two types of the On and Off source areas described below.

2.1 Analysis for Super Galactic Plane (SGP)

The Super Galactic Plane (SGP) is a plane which contains more nearby galaxies of our Local Group [6]. The Exposure in TA experiment is almost equally divided when we define a sky within ±30° of SGP as the On source area, and the other as the Off source area. The fraction of the exposure for the On and Off source areas to the total exposure are 52% and 48% respectively. The distributions of zenith angles of air-shower events for the On and Off source areas are plotted in Fig.2. First we compare the energy distributions of observed air shower events from this On and Off source areas. Fig.3 shows the energy distributions of the observed showers obtained for entire exposure, On and Off source areas. The shape of the distributions were evaluated by maximum likelihood fit with broken power law. The black line in Fig. 3 shows the best fit broken power law expressed by Eq. 2.1. Here E_o is 1EeV. C_0 represents the normalization constant promotional to total number of events. The values $\alpha_{1,2}$ represent spectrum index below the energy E_b and above E_b respectively.

$$\frac{\Delta N(E)}{\Delta \log_{10}\left(\frac{E}{E_o}\right)} = C_0 \left(\varepsilon\left(E,E_b\right)\left(\frac{E}{E_o}\right)^{-\alpha_1} + \left(1-\varepsilon\left(E,E_b\right)\right)\left(\frac{E}{E_o}\right)^{-\alpha_2} \right) \tag{2.1}$$

$$\varepsilon(E,E_b) = \{\, 1 : (E < E_b)\ , 0 : (E > E_b) \tag{2.2}$$

The Best fit parameters for energy distribution obtained from the entire exposure are $C_o = 2.141^{+0.343}_{-0.298} \times 10^{+4}$, $\alpha_1 = -1.775^{+0.053}_{-0.053}$, $\log_{10}(E_b/EeV) = 1.778^{+0.040}_{-0.068}$ and $\alpha_2 = -3.910^{+0.643}_{-0.660}$. The difference of the shapes of the energy distribution between the On and Off source areas is expected to be visible when we see the broken energy and the event fraction above the energy. So while we evaluate energy distribution from On source and Off source, α_1 is set to the value obtained from the fit to the distribution for the entire exposure. The C_0 is set to the value multiplying the fraction of exposure. $\log_{10}(E_b/Eo)$ and α_2 are set free and obtained for On and Off source areas. The obtained broken power law function is plotted in Fig.3 as solid and dashed lines. Error contour for obtained parameters are drown in Fig.3 as red and blue lines. Table.1 shows summarized best fit parameters and errors. There are difference in break energy between On source and Off source area. The difference, $\Delta\log_{10}(E_b/E_o)$ is 0.16. The event fraction of the Off source area to the On source area above the break energy $(N_{off}(E > E_b)/N_{on}(E > E_b))$ is 0.34 instead of 0.48 which is expected from the exposure ratio. The chance probability was estimated by a simulation assuming both distribution are coming from population which is same with entire exposure's one. The estimation were done by simple Monte Carlo simulation which is shuffling entire event in each energy bin to On source and Off source distribution according to the fraction of exposure binomially. At each trial of simulation, we obtain a random distribution coming from the same population, and did same evaluation for the distribution difference. Fig. 5 shows the frequency distribution. The horizontal axis corresponds to "Off source" 's break energy and vertical axis corresponds to event fraction above the break energy. Table. 2 shows chance probability to obtain each case. The observed value correspond to a probability $\sim 0.62 \times 10^{-4}$ (3.2σ).

Area	C_o	α_1	$\log_{10}(E_b/EeV)$	α_2
All	$2.141^{+0.343}_{-0.298} \times 10^{+4}$	$-1.775^{+0.053}_{-0.053}$	$1.778^{+0.040}_{-0.068}$	$-3.910^{+0.643}_{-0.660}$
On source	$(1.1128 \times 10^{+4})$	(-1.775)	$1.832^{+0.069}_{-0.041}$	$-3.910^{+0.696}_{-1.260}$
Off source	$(1.0286 \times 10^{+4})$	(-1.775)	$1.668^{+0.052}_{-0.053}$	$-3.858^{+0.582}_{-0.818}$

Table 1: The best fit broken power law parameters measured by three energy distributions from the whole area, On source and Off source area.

2.2 Analysis for the known object list (VCV list)

The object list used in this analysis is Veron-Chetty& Veron 12 catalogue with z<0.018 [7]. This is same object list and the criteria for objects already used at other correlation study [8]. The definition of On source area and Off source area is searched by changing the size of opening

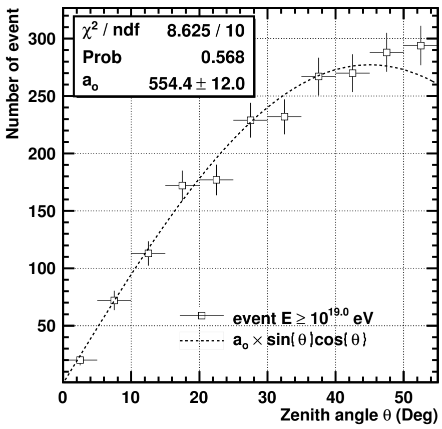

Figure 1: The zenith angle distribution of observed shower event with energy E $\geq$ 10 EeV.

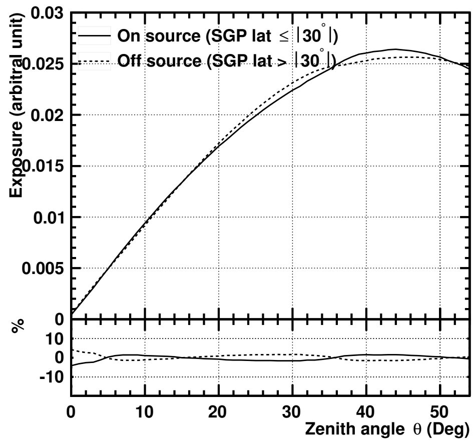

Figure 2: The zenith angle distributions while observing the On source area and Off source areas

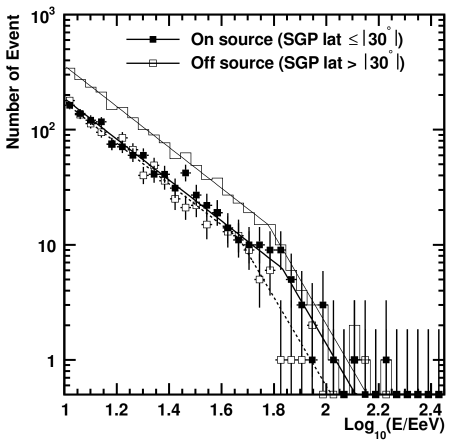

Figure 3: The energy distributions of observed shower events for the On/Off areas using SGP. The black histogram shows entire events. The ■ and the □ points show energy distribution observed from On source area and Off source area respectively.

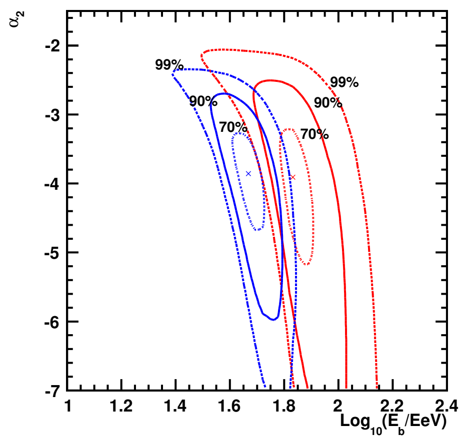

Figure 4: Contour of $\delta \log L$ on the plane of two parameters (E_b and α_2). Contour levels are drawn at 70%,90% and 99% level. Blue and red contours denote the confidence levels for the Off and On source areas respectively.

angle from 1° to 15° to maximize deviation. While deciding opening angle, we introduce a plot named as “fraction plot”.Fraction plot is a plot of fraction of event at “On source area” and “Off source area” as a function of a energy. If the two energy distributions come from same population, the fraction should obey binomial probability of population rate calculated from exposure. The largest deviation from the exposure ratio was seen in data at the case the opening angle is 11°. The exposure fractions are 0.81 and 0.19 for On source and Off source areas, respectively. The zenith angle distributions while observing On source area and off source area is plotted in Fig. 7. The exposure for On and Off source area have only small deviation from geometrical exposure. Fig. 6 shows the event fraction at Off source area when 11° is the opening angle for On source

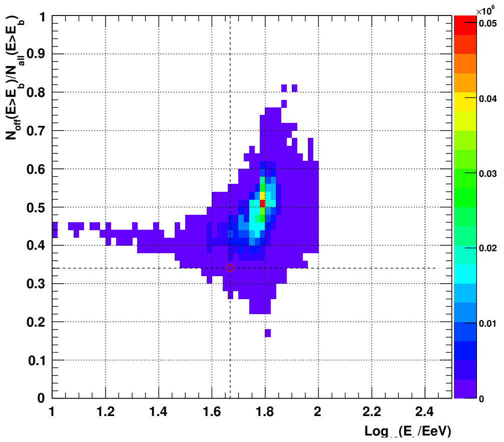

Figure 5: The plot of the event fraction above the break energy versus $\log_{10}(E_b/EeV)$ for the Off source area using random Monte Carlo simulation.

area	Case	Fraction
$E_b > 10^{1.668}EeV, \frac{N_{off}(E>E_b)}{N_{on}(E>E_b)} > 0.34$	41580	0.83177
$E_b > 10^{1.668}EeV, \frac{N_{off}(E>E_b)}{N_{on}(E>E_b)} < 0.34$	7996	0.15996
$E_b < 10^{1.668}EeV, \frac{N_{off}(E>E_b)}{N_{on}(E>E_b)} < 0.34$	31	0.00062
$E_b < 10^{1.668}EeV, \frac{N_{off}(E>E_b)}{N_{on}(E>E_b)} > 0.34$	383	0.007662

Table 2: The number of cases for the areas described in the left column in the random simulation. The estimated chance probability to obtain larger deviation is 6.2×10^{-4}.

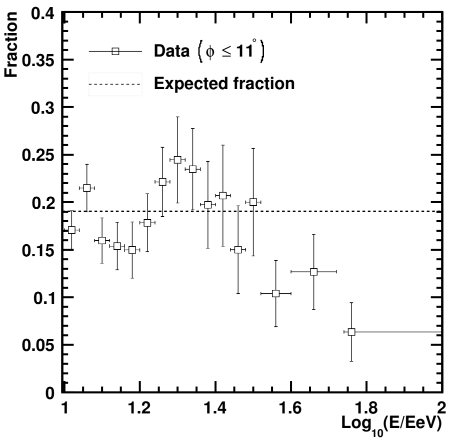

Figure 6: The event fraction for the Off source area as a function of energy. The open squares are the observed data and the dotted line is the expected fraction.

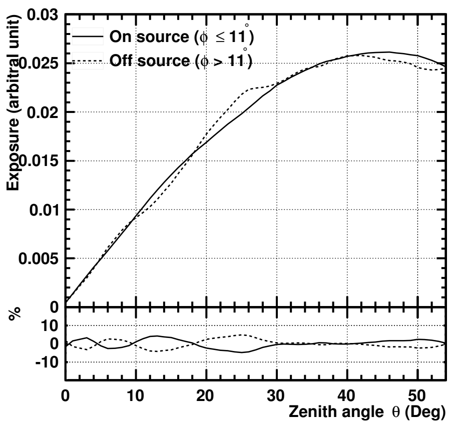

Figure 7: The zenith angle distribution while observing On source area and off source area.

area. Fig. 8 shows the energy distribution obtained from entire exposure, On source area and Off source area.The error contour obtained for the best fit parameters are shown in Fig. 9. The best fit parameters are summarised in Table. 3. There is a difference in the break energies between the On source area and the Off source area by $\Delta\log_{10}(E_b/E_o) \sim 0.31$. And the event fraction at Off source area above the break energy $(N_{off}(E > E_b)/N_{on}(E > E_b))$ is 0.12 instead of 0.19 which is expected from the exposure ratio. As showin in Fig. 10 and Table. 4, the chance probability was estimated using the same procedure that was applied for the SGP analysis. A penalty factor for the estimated probability was calculated by counting the relative frequency of the best opening angle in Monte Carlo simulation. The estimated penalty factor is 9.

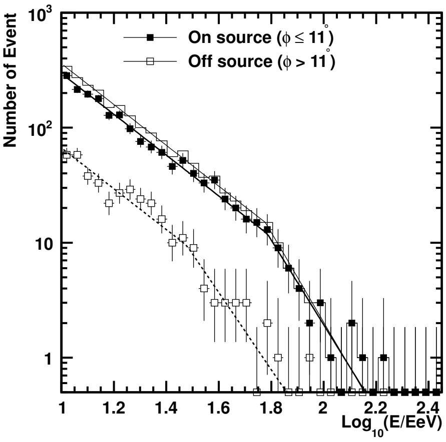

Figure 8: The energy distributions of observed shower events for the On/Off areas using AGN. The black histogram shows entire events. The ■ and the □ points show energy distribution observed from On source area and Off source area respectively.

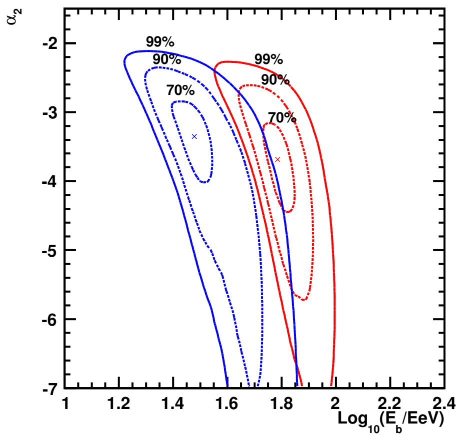

Figure 9: Contour of $\delta \log L$ on the plane of two parameters (E_b and α_2). Contour levels are drawn at 70%,90% and 99% level. Blue and red contours denote the confidence levels for the Off and On source areas respectively.

Area	C_o	α_1	$\log_{10}(E_b/EeV)$	α_2
All	$2.141^{+0.343}_{-0.298} \times 10^{+4}$	$-1.775^{+0.053}_{-0.053}$	$1.778^{+0.040}_{-0.068}$	$-3.910^{+0.643}_{-0.660}$
On source	$(1.7336 \times 10^{+4})$	(-1.775)	$1.786^{+0.058}_{-0.046}$	$-3.663^{+0.515}_{-0.784}$
Off source	$(4.0782 \times 10^{+4})$	(-1.775)	$1.470^{+0.061}_{-0.084}$	$-3.352^{+0.529}_{-0.673}$

Table 3: The best fit broken power law parameters measured by three energy distributions from the whole area, On source and Off source area defined using AGNs.

2.3 Systematic error

As showin in Fig.2 and Fig.7, the observing condition is not significantly differ as compared to large statistical error at high energy tail of distribution which is currently interested in. So this comparison does not affect the systematic uncertainty of zenith angle dependence of energy estimator obtained from Monte Carlo simulation. The duty cycle of the observation with the surface detector is also more than 95% constantly for over 5 years. To make sure the remaining effect of time variation of energy scale due to atmospheric condition which is supposed to be averaged for over 5 years, the rate of reconstructed events with energies greater than $10^{19.0}$ eV was collected in anti-sidereal time [9] and checked. The fluctuation amplitude of the event rate in the time bin is at most 5% ±3%. Considering spectrum index at around $10^{19.0}$ eV, this corresponds to the energy shift by 2.5% if we assume this amplitude is caused by a systematic effect from remaining variation of energy scale. After considering this shift, chance probability for the SGP analysis is still 6.9×10^{-4} (3.2 σ).

3. Summary and discussion

In this analysis, the new approach to search for the anisotropy of UHECR is developed and

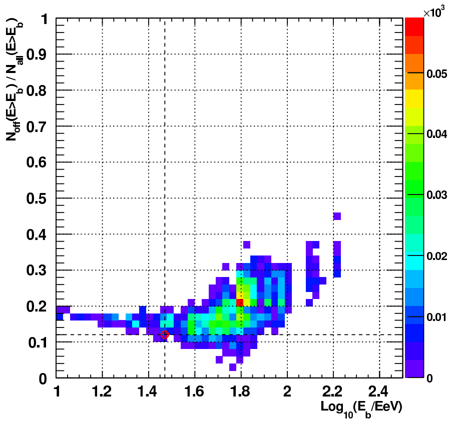

Figure 10: The plot of the event fraction above the break energy versus $\log_{10}(E_b/EeV)$ for the Off source area using AGNs in the VCV catalogue at the random Monte Carlo simulation.

area	Case	Fraction
$E_b > 10^{1.470}EeV, \frac{N_{off}(E>E_b)}{N_{on}(E>E_b)} > 0.12$	2004	0.845
$E_b > 10^{1.470}EeV, \frac{N_{off}(E>E_b)}{N_{on}(E>E_b)} < 0.12$	213	0.090
$E_b < 10^{1.470}EeV, \frac{N_{off}(E>E_b)}{N_{on}(E>E_b)} < 0.12$	4	1.7×10^{-3}
$E_b < 10^{1.470}EeV, \frac{N_{off}(E>E_b)}{N_{on}(E>E_b)} > 0.12$	152	0.0064

Table 4: The number of cases for the condition described in the left column in the random simulation.

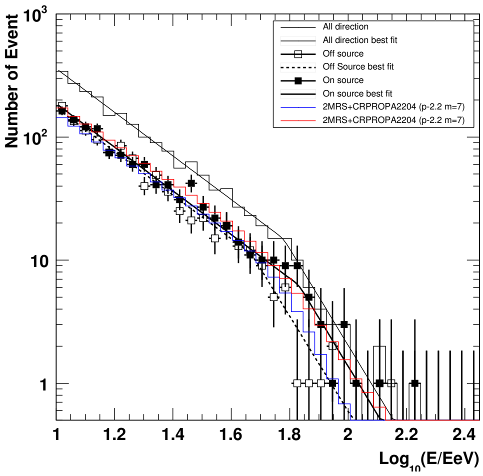

Figure 11: Comparison of energy distributions expected for protons arriving from the sources with power index of -2.2, evolution parameter of 7 and 2MRS density profile.

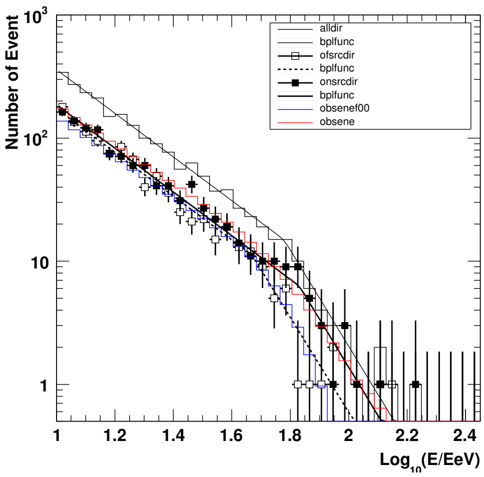

Figure 12: Same figure with Fig. 16 with artificial cut on source distribution at off source side <75Mpc.

employed, which considers the mechanism of modulation of energy spectrum due to an energy loss of particles in CMB during the propagation. The energy distributions of observed events were evaluated with break energy obtained from broken power low fit and event fraction above the break energy. Observed energy distribution within 30° from SGP and out were compared. The result is summarised in Table. 1. Chance probability is estimated as $\sim 6.2 \times 10^{-4}$ (3.2σ) using binomial Monte Carlo simulation as shown in Fig. 5. Also Observed energy distribution within 11° from VCV agn object and out were compared. The result is summarised in Table. 3. Chance probability is estimated as $\sim 1.5 \times 10^{-2}$ (2.2σ) after considering penalty factor for the scan of opening angle.

Off source flux shows steeper suppression than the one from On source area. To make sure the feature of the observed energy distributions, we performed simulation using a propagation code CRPropa2.2.0.4 [10] and the source distribution from the object density of 2MRS catalogue [11] using the density profile calculation described in [12]. Fig. 11 and Fig. 12 display results simulated energy distribution of cosmic ray. Here the source spectrum index and evolution parameter along red shift were set at -2.2 and 7, respectively [13]. Qualitatively, The difference of observed energy distributions between the On source and Off source areas was reproduced well by simulation. We conclude there is difference in flux attenuation of cosmic ray in northern hemisphere and the approach with this study will help to investigate cosmic ray source model and chemical composition. We will look for the best source model and/or chemical composition model by this approach further in detail by increasing statistics of observed cosmic ray.

4. Acknowledgements

The Telescope Array collaborators and acknowledgement is listed in the URL in foot note[1].

References

[1] K. Greisen, , *Physical Review Letters* **16** (Apr., 1966) 748–750.

[2] G. T. Zatsepin and V. A. Kuz'min *Soviet Journal of Experimental and Theoretical Physics Letters* **4** (Aug., 1966) 78.

[3] T. Abu-Zayyad et al., *The cosmic-ray energy spectrum observed with the surface detector of the telescope array experiment*, *The Astrophysical Journal Letters* **768** (2013), no. 1 L1.

[4] T. Abu-Zayyad et al. *Nuclear Instruments and Methods in Physics Research Section A: Accelerators, Spectrometers, Detectors and Associated Equipment* **689** (2012), no. 0 87 – 97.

[5] Telescope Array Collaboration, , *ArXiv e-prints* (Mar., 2014) [arXiv:1403.0644].

[6] G. de Vaucouleurs, , *aj* **58** (Feb., 1953) 30.

[7] M.-P. Véron-Cetty and P. Véron, , *Astronomy and Astrophysics* **455** (Aug., 2006) 773–777.

[8] J. M. Neto and the Pierre Auger Collaboration *Journal of Physics: Conference Series* **409** (2013), no. 1 012108.

[9] F. J. M. Farley and J. R. Storey *Proceedings of the Physical Society. Section A* **67** (1954), no. 11 996.

[10] K.-H. Kampert, J. Kulbartz, L. Maccione, N. Nierstenhoefer, P. Schiffer, G. Sigl, and A. R. van Vliet *Astroparticle Physics* **42** (2013), no. 0 41 – 51.

[11] J. P. Huchra et al. *The Astrophysical Journal Supplement Series* **199** (2012), no. 2 26.

[12] H. B. J. Koers and P. Tinyakov *Monthly Notices of the Royal Astronomical Society* **399** (2009), no. 2 1005–1011, [http://mnras.oxfordjournals.org/content/399/2/1005.full.pdf+html].

[13] E.Kido et al. *Proceedings of UHECR2014 conference* (2014).

[1] http://www.telescopearray.org/images/papers/ICRC2015-authorlist.pdf